Source parameters estimation of reservoir-induced earthquakes in northeastern Brazil using Empirical Green´s Function analysis

Jelena Tomic (UCLA), Rachel E. Abercrombie (Boston University) and Aderson F. do Nascimento, (DFTE/PPGG/UFRN)

Abstract

In the Açu dam area (NE Brazil), a digital seismograph local network was deployed for nearly three years and recorded one of the best examples of Reservoir-induced seismicity on a near-homogeneous Precambrian crystalline basement. The hypocentral error location are approximately 100m and are very suitable for investigating a possible relationship between pore-pressure diffusion and source parameters like stress drop, rupture velocity, source duration and rupture length. In order to obtain these source parameters from recorded seismograms, attenuation and site effects have to be removed. Empirical Green´s Functions (EGF) is an alternative way to extract the earthquake source information from the recorded digital seismograms. Here we present results from EGF analysis of 6 earthquakes in the Açu dam area. Estimates of source duration and corner frequency imply low stress drop (10 to 100 MPa) for these shallow reservoir-induced seismicity events. These are similar to tectonic earthquakes, suggesting that hypocentral depths and the presence of water do not affect stress drop.

Introduction

During the last 50 years both theoretical models and observations have clearly shown the correlation between the change in local stress and/or the increase in pore pressure along faults (see Gupta, 1992). Abercrombie and Leary (1993) showed that the stress drops (difference in stress on the fault plane before and after an earthquake) of small, induced earthquakes (seismic moment < 10^{14} Nm) seems to be systematically lower than those of tectonic earthquakes of similar magnitude (Figure 1). Stress drop ($\Delta\sigma$) is one of the source parameters directly related to the ground acceleration produced by an earthquake, hence resolving the stress drop controversy between natural and induced earthquakes can lead to better understanding of the physics of earthquake source processes and prediction of the seismic hazard. Stress drop values are heavily dependent on the choice of source model used, and the assumption of constant rupture velocity that is necessary to calculate the area ruptured by the earthquake. The goal of this study is to put quantitative constraints on values of stress drop and rupture velocity by employing EGF analysis on a high quality data set of reservoir-induced earthquakes from Açu Reservoir, NE Brazil. Other methods have been used to estimate source parameters for these earthquakes (Tomic et al, 2006) Static stress drop ($\Delta\sigma$) is the difference in stress on the fault plane before and after the earthquake (Brune, 1970). For a circular crack, $\Delta\sigma$ is estimated following Eshelby (1957):

$$\Delta\sigma = \frac{7M_0}{16r^3} \quad (1)$$

where M_0 is the seismic moment (Nm), and r is the source radius (m). The total duration of slip on the fault is proportional to the duration of the pulse recorded on the seismogram (Madariaga, 1976). When converted into the frequency domain, the finite pulse duration produces a corner frequency (f_c) in the displacement spectrum. Thus, the corner frequency can also be used to estimate the earthquake rupture size. Seismic moment is also proportional to the area under the displacement pulse, and thus also the long period amplitude of the displacement spectrum. As implied by equation (1), any uncertainty in the source radius becomes cubed in the stress drop. The uncertainties in determining the radius of the earthquake rupture and consequently the stress drop from standard frequency domain analysis, are a combination of data quality, analysis techniques and assumed source models. Studies by Archuleta (1986) found an increase in $\Delta\sigma$ with increasing moment for M_0 < 10^{14} Nm implying a breakdown in scaling of earthquake rupture process with the earthquake size. Using earthquakes recorded at 2.5 km depth, Abercrombie (1995) demonstrated unambiguously that seismic noise and near surface attenuation severely bias stress drop estimates made from the surface recording. Another uncertainty in the stress drop determination comes from the difference in the source models used. The Brune (1970), and Madariaga (1976) are simplistic circular crack source models commonly used. The Brune model assumes a circular fault rupturing instantaneously in the medium, while in the Madariaga model rupture nucleates at a point and propagates outward reaching a certain diameter when the propagation simultaneously stops. The difference in the fault radius estimate using Madariaga or Brune circular crack models is a factor of 1.76, resulting in the stress drop difference of almost a factor of 6. Thus, the uncertainty in the stress drop estimate is strongly dependent on the source model used to convert the corner frequency into the source dimension. Abercrombie & Leary (1993) and Abercrombie (1995) observed the predicted cubic relation between seismic moment and earthquake source radius, and hence a constant stress

drop for naturally occurring earthquakes covering a moment range of 20 orders of magnitude. However, induced earthquakes appear to have systematically lower stress drops than the tectonic earthquakes. Studies by Fehler and Phillips (1991), and Gibowicz *et al.* (1991) that analyzed earthquakes induced by hydro-fracturing and coring respectively, estimated stress drops that are on average one order of magnitude lower than those of naturally occurring earthquakes. Induced seismicity is usually much shallower than the tectonic seismicity implying the amount of normal load might be directly affecting the amount of stress drop. In the case of reservoir-induced earthquakes and hydro-fractures there is an excessive amount of water associated with faulting perhaps providing another clue into what affects the amount of stress drop. As noted above, the uncertainty in measurements of the stress drops is several orders of magnitude, thus the apparent shift in stress drop of induced earthquakes could be an artifact of models used, or a consequence of a different tectonic setting or other environmental condition.

In the following sections we use EGF analysis to estimate source parameters of 6 earthquakes ($1.8 \leq M_w \leq 2.2$) induced by impoundment of the Açu Reservoir, NE Brazil. Results of this study show stress drops in the range of 10 to 100 MPa and a rupture velocity of at least 0.6 β, where β is the shear wave velocity, indicating that reservoir-induced earthquakes are comparable to naturally occurring earthquakes.

Geological Setting and Background on the site

The study area is located on the eastern continental margin of the South American plate. The region lies in the Precambrian (>540 Ma) crystalline basement approaching a Cretaceous-Cenozoic sedimentary basin. The crystalline basement is composed of the Caico´ (predominantly gneisses and mig-matites) and the Serido´ groups (predominantly mica-schists, marbles, and quartzites). Açu reservoir was constructed in 1983 and has a capacity of 2.4×10^9 m^3 maintained by a 34 m high earth-filled dam constructed on Precambrian shield. Annual reservoir variation is 3-6 m which results in annual seismic activity due to a proposed mechanism of pore pressure diffusion (Ferreira *et al.* (1995), do Nascimento *et al.* (2004). Digital data at Açu have revealed the seismic activity in remarkable detail (do Nascimento *et al.* 2004). The majority of earthquake activity is clustered within several well-defined zones and individual zones are active over discrete periods of time. It has also been shown that the observed spatial and temporal evolution of seismicity at Açu is defined by pressure diffusion through local fault planes with heterogeneous permeability structures do Nascimento *et al.* (2005a,b).

Induced seismic activity in the Açu area has been monitored over a ten year period from 1987-1997. However, accurate hypocentral information is only available from 1994 to 1997, when a network of three-component digital seismographs were operational which have provided a very accurate assessment of hypocentral with errors of ≈100m do Nascimento *et al.* 2004. This high-quality dataset is here used to estimate source parameters from EGF analysis.

Methodology

In order to calculate source dimensions we use EGF analysis in both the frequency and time domains. This analysis is based on the assumption that a small, collocated seismic event can be deconvolved from the earthquake of interest, so that one cancels out site and path effects, providing an "unbiased" estimate of the source size (Hough, 1997). The EGF analysis works best if the seismic moment of the largest event is at least one order of magnitude greater than the small earthquake and both have the same focal mechanism. When these conditions are fulfilled, the small seismic event is named the "Green function" of the larger seismic event.

Source parameters from Spectral Ratios

We fit all the spectral ratios in a group solving for two corner frequencies and the ratio of Moments of the earthquake pair assuming the ω^{-2} source model:

$$A(f) = \frac{\Omega_{O(big)}\left[1+(f/f_{c(small)})^{n\gamma}\right]^{1/\gamma}}{\Omega_{O(small)}\left[1+(f/f_{c(big)})^{n\gamma}\right]^{1/\gamma}} \quad (2)$$

where f_{cbig} and f_{csmall} are the corner frequencies of the large and small earthquakes, respectively. Because of our limited bandwidth, the small earthquake f_c is not resolved in most cases. Rather than simply choosing one EGF as best, or averaging the results of all, spectral ratios are stacked to obtain an average geometric mean of the source spectrum (Figure 3). To make the best estimate of the large earthquake corner frequency we consider a choice of EGF according to the criteria: (1) long period amplitude ratio higher than 10 (this provides the needed magnitude difference), (2) fit to spectral ratios converged, (3) quality of time domain source time function. To ensure that only the part of the spectral ratio resulting from the large earthquake is included we select a frequency range ending well below the corner frequency of the small earthquake. Since the small earthquake corner frequency is typically too high to be resolved I predict it using the long period amplitude ratio and assuming that both large and small earthquake have the same stress drop. From equation (1) (Eshelby, 1957), it follows that:

$$f_{c(small)} = f_{c(big)}\left(\frac{\Omega_{O(big)}}{\Omega_{O(small)}}\right)^{\frac{1}{3}} \quad (3)$$

We only include the frequency range up to 80% of the predicted $f_{c(small)}$ for individual ratios in the mean. In virtually all the cases where amplitude ratio is greater than 10 this limit is higher than 60 Hz which we consider the highest resolvable frequency (80% of the Nyquist frequency). I stack together all the "successful" ratios in their chosen frequency range to calculate a geometric mean source spectrum for the large earthquake (Figure 3). Then, we fit the spectral ratio using equation (3) with $e^{-\pi ft/Q} = 1$ solving for the f_{cbig} for N and E channel individually. I then calculate the vector sum of the mean

displacement spectra on the two channels: $\overline{A}(f) = \sqrt{(A_N(f))^2 K + (A_E(f))^2}$ (4)

where $\bar{A}$ is the vector sum of the mean spectral ratios, A_N and A_E are the mean displacement spectra on the North and East components respectively, and K is the long period amplitude ratio between N and E for the largest earthquake. Multiplying by K ensures that energy distribution on each channel is preserved.

Fitting this vector sum of the mean spectral ratios for the $f_{c(big)}$ is then our best estimate of the actual source spectrum of the large earthquake. Figures 2 and 3 show the mean spectral ratios of individual channels for all earthquakes and the mean of both.

Attenuation Estimates from EGF Spectral Ratios

If spectra obtained by deconvolution are true source spectra, then by dividing the individual spectrum of the large earthquake by its source I can estimate the spectrum of the attenuation. I fit the attenuation spectrum with: $Atten(f) = A_0 e^{-\pi f \frac{t}{Q}}$ (5)

where A_0 is the long period level, and f is the frequency range. The mean value for all the stations from all spectral ratios used is 232, remarkably similar to the Q estimates obtained by the individual spectra fitting (Q=227).

Source Parameters from the Source Time Functions

We also estimate an average source time function pulse for each station by picking the best individual pulses in the group on all 3 components, and calculating the mean. I measure the total duration of the pulse from the first to second zero crossing (Figure 4). Since the pulse does not have sharp onsets, an error is introduced in the estimation of the pulse duration. The duration of the pulse should be inversely proportional to the corner frequency. For a symmetric triangular pulse, the pulse duration scales as $1/\pi$ times the inverse of the corner frequency. As specified by Boatwright (1980) the source radius (r) relates to the rise time: $r = \frac{\tau_{1/2} v}{1 - \frac{v}{c}\sin\theta}$ (6), where r is the source radius, $\tau_{1/2}$ is the rise time of the pulse, c is the S wave velocity, v is assumed to be 0.9 times the S wave velocity as in frequency domain analysis, and θ is the take off angle with respect to the fault normal. In the Açu data the pulses are symmetrical and the measurements of the rise time are directly proportional to the total pulse duration for all θ. Such pulse symmetry is not the case in Boatwright's (1980) model, where rise times are inversely proportional to the total pulse durations. Hence the correction for θ does not appear to be correct for our earthquakes. To calculate the source radius, I determine θ for each station assuming the composite focal mechanism (do Nascimento, 2004), and also assume a constant θ of 45° following Frankel and Kanamori (1983). Our resolution limit is approximately 0.025 sec. The application of the Boatwright model in this study results in very low stress drop estimates (0.1 to 1 MPa) for both choices of θ.

Rupture Velocity

To calculate the earthquake source radius and stress drop from the corner frequency almost all previous studies of small earthquakes assume a rupture velocity in the range of 0.6 to 0.9β (Brune, 1970; Fehler and Phillips, 1991; Abercrombie, 1995) . Boatwright (1980) shows that for rupture velocities greater than half the shear wave velocity, pulse shapes and spectra vary over the focal sphere even if a simple circular rupture is assumed. If the rupture is unilateral, the variation in the pulse width or corner frequency will be even larger making it possible to estimate rupture velocity from the pulse width variations. The recorded pulse width is the largest at stations lying 180° from the rupture direction, and the shortest at the stations in direction of the rupture propagation, for a unilaterally propagating rupture (Aki and Richards, 1980).Following Frankel and Kanamori (1983), we perform a directivity analysis using the measured pulse widths: $\delta t = t_o - \Gamma\Delta$ (7), where δt is the pulse width (sec), t_o is the rupture duration, Δ is the horizontal distance between start and end of the earthquake, and Γ is the directivity parameter ($\Gamma = cos(\varphi)/c$, where φ is the fault-to-station azimuth, and c is the wave phase velocity). We use the S wave velocity of 3150 m/s and assume that the earthquake rupture is confined to the fault plane striking N45° (do Nascimento, 2004). By fitting the directivity parameter against the pulse width at each station we have estimated the rupture velocity for each of the 6 earthquakes (see an example in Figure 5). Equation (7) is valid for purely unilateral ruptures. If an earthquake ruptures at all bilaterally, there will be less variation in the pulse width along the azimuth. This will result in an underestimation of the rupture velocity (equation 7) The limiting case is a purely bilateral rupture that results in V_r = 0. For smaller earthquakes (M < 2) the limited digitization rate under samples the displacement pulses also resulting in the very low rupture velocity (0.02 to 0.07 β). Earthquakes in Figure 5 show clear azimuthal variation in the pulse width corresponding to a unilateral rupture. Not all the events involve a unilateral rupture, showing no azimuthal dependence on the pulse width, and resulting in an unrealistically low rupture velocity (0.06β). This analysis allows me to calculate a rupture length for the earthquakes with clear unilateral propagation. I then calculate stress drop from the source length using Kanamori and Anderson's (1975) relation for a unilateral strike slip fault:

$$\Delta\sigma = \frac{2M_0}{\pi w^2 L}$$

where $\Delta\sigma$ is the stress drop, M_0 is seismic moment estimated from the standard frequency domain analysis (single spectrum), L is the rupture length and w is the rupture width. We assumed two different values for the estimated width: $L/2$ and $L/10$ and. The first give stress drops estimates between 10 and 100 MPa. The latter one

gives very high stress drop (>100 MPa) and stands out from all other estimated values.

Conclusions

From the study using EGF analysis we have concluded that:

- Stress drops of reservoir induced earthquakes are not systematically lower than those of similar sized tectonic events (between 10 and 100 MPa);
- The difference between source models used to calculate source parameters is larger than the difference produced using common methods such as fitting of individual spectra and the Empirical Green's function deconvolution;
- The small earthquakes have rupture velocities of $\geq 0.6\beta$, similar to those of large tectonic earthquakes justifying previous assumptions;
- Small earthquakes also show directivity;
- The mean value for *Q* for all the stations from all spectral ratios used is 232 – very similar to the *Q* estimates from fitting individual spectra (*Q*=227).

Acknowledgements

We wish to thank NSF and CNPq for financial support.

Referências

Abercrombie, R. E., Earthquake Source Scaling Relationships From -1 to 5 M_L Using Seismograms Recorded at 2.5-km Depth. 1995. *Journal of Geophysical Research.*, 100, 24,015-24,036.

Abercrombie, R. E., and P. Leary, 1995. Source Parameters of Small Earthquakes Recorded at 2.5 km Depth, Cajon Pass, Southern California: Implications for Earthquake Scaling, *Geophysical Research Letters,* 20, 1511-1514.

Aki, K., and P. Richards, Quantitative Seismology. 1980. 932, pp., W. H. Freeman, New York.

Archuleta, R. J., Downhole recording of seismic radiation, *Earthquake Source Mechanics. 1986.* Maurice Ewing Series, 6, by S. Das, J. Boatwright, and C H. Scholz, Editors, American Geophysical Union, Washington, DC., 319-329.

Boatwright, J., A Spectral Theory for Circular Seismic Sources; Simple Estimates of Source Dimension, Dynamic Stress Drop, and Radiated Seismic Energy, . 1980. *Bulletin of the Seismological Society of America,* 70, 1-27..

Brune, J., Tectonic Stress and the Spectra of Seismic Shear Waves from Earthquakes, 1970. *Journal of Geophysical Research.,*75, 4,997-5009.

Eshelby, J. D., The Determination of the Elastic of an Ellipsoidal Inclusion and Related Problems. 1957. *Proceedings of the Royal Society of London, A, 241*, 376-396.

do Nascimento, A. F., P. A. Cowie, R. J. Lunn, and R. G. Pearce. 2004. Spatio-temporal evolution of induced seismicity at Ac¸u reservoir, NE Brazil, Geophys. J. Int., 158, 1041 – 1052, doi:0.1111/j.1365-246X. 2004.02351.x.

do Nascimento, A. F., R. J. Lunn, and P. A. Cowie. 2005a., Numerical modelling of pore pressure diffusion in a reservoir-induced seismicity site in northeast Brazil, Geophys. J. Int., 160, 249–262.

do Nascimento, A. F., R. J. Lunn, and P. A. Cowie. 2005b. Modelling the heterogeneous hydraulic properties of faults using constraints from reservoir-induced seismicity . J. Geophys. Res., 110, B09201, doi:10.1029/2004JB003398.

Fehler, M., and W. S. Phillips, Simultaneous Inversion for *Q* and Source Parameters of Microearthquakes Accompanying Hydraulic Fracturing in Granitic Rock. 1991. *Bulletin of the Seismological Society of America,* 81, 553-575.

Frankel, A., and H. Kanamori, Determination of Rupture Duration and Stress Drop for Earthquakes in Southern California. 1983. *Bulletin of the Seismological Society of America*, 73, 1527-1551.

Gibowicz, S. J. R. P. Young, S. Talebi, and D. J. Rawlence, Source Parameters of Seismic Events at the Underground Research Laboratory in Manitoba, Canada: Scaling Relations for Events with Moment Magnitude Smaller Than -2. 1991. *Bulletin of the Seismological Society of America,* 81, 1157-1182.

Gupta, H. K., Reservoir-Induced Earthquakes, *Elsevier*, Amsterdam, 364, 1992.

Hough, S. E., Empirical Green's Function Analysis; Taking the Next Step. 1997. J. Geophys. Res., B, Solid Earth and Planets, 85, 1576-1590.

Kanamori, H., and D. L. Anderson, Theoretical Basis of Some Empirical Relations in Seismology. 1975. *Bulletin of the Seismological Society of America,* 65, 1073-1095.

Tomic, J, Abercrombie, R. E., do Nascimento, 2006. Source Parameters and Rupture Velocity of Small M≤2.2 Reservoir Induced Earthquakes. In preparation for Geophys. Res. Let.

Madariaga, R., Dynamics of an Expanding Circular Fault, 1976. *Bulletin of the Seismological Society of America,* 66, 639-666.

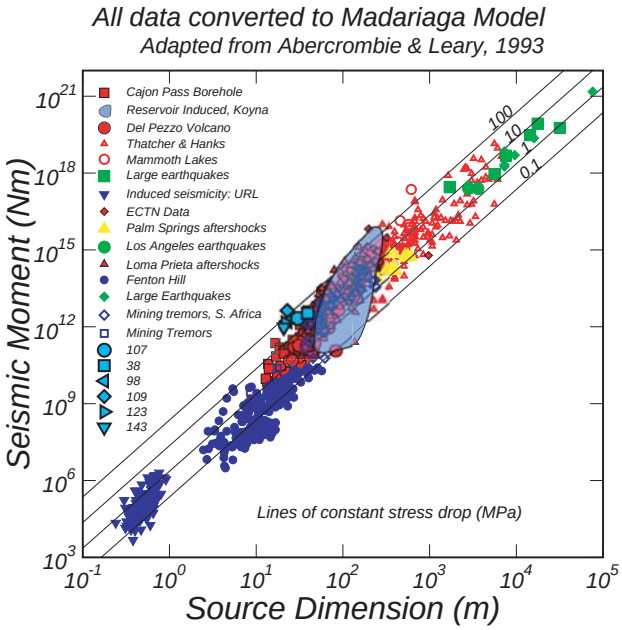

Figure 1: composite plot adapted from Abercrombie and Leary (1993) showing seismic moment versus source radius for several studies. All the results are converted to the Madariaga (1980 model) for better comparison. Solid lines represent constant stress drop calculated following Eshelby (1957). Blue symbols represent induced earthquakes. Low stress drop earthquakes: dark blue circles induced by hydraulic fracturing (Fehler and Phillips, 1991), blue triangles induced by shaft excavation (Gibowicz et al. 1991), transparent blue area are reservoir induced earthquakes at Koyna, India (Mandal, *et al*., 1998). This study: earthquakes 107 through 143 are the six largest earthquakes.

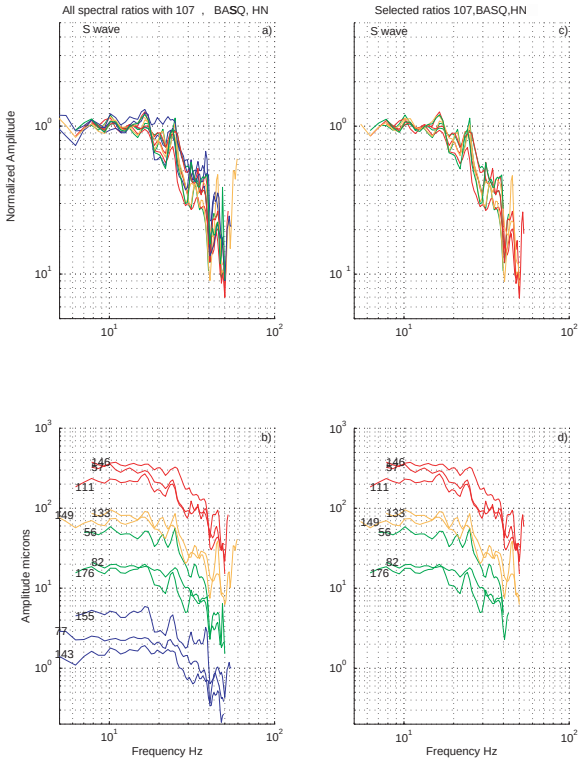

Figure 2: Empirical Green's Function in frequency domain. S wave spectral ratios for a group of collocated events at station BASQ. Left column (graphs a, and b) show the entire group of earthquakes. Right column illustrates the selected spectral ratios that comprise the average 107 source spectrum.

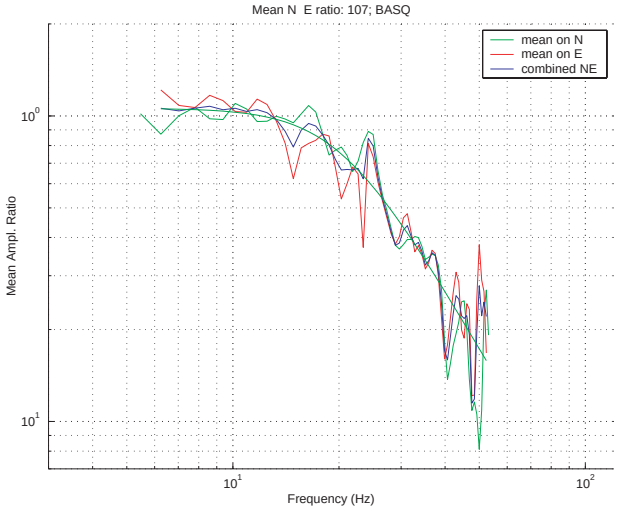

Figure 3: Correlation of mean source spectrum for earthquake 107. Example of the mean source spectrum from channel N and E. Blue line is the mean for both channels corrected for the amplitude ratio between them.

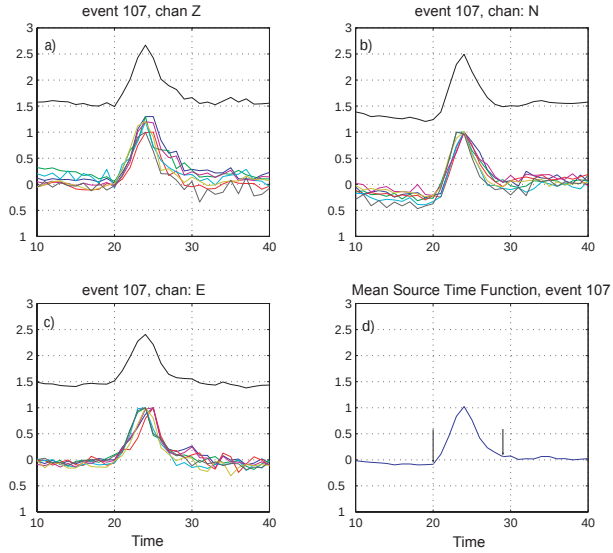

Figure 4: Mean Source Time Function for earthquake 107. a) b) and c) The top black line is the mean of all the EGF pares picked (bottom) for channels Z, N, and E respectively. d) Mean source time function of earthquake 107 of all channels. The arrows indicate the pick of the onset and the end of the pulse.

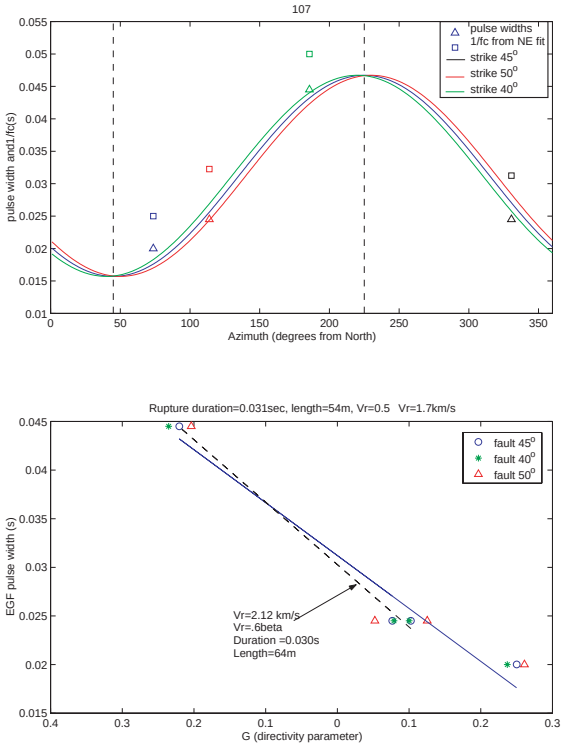

Figure 5: Directivity, earthquake 107. Rupture Velocity: variation in pulse width azimuth: The top graph of figures (12) through (18) shows the variation in the pulse width with the station azimuth.